ELSEVIER

Journal of Crystal Growth 227–228 (2001) 545–552

JOURNAL OF CRYSTAL GROWTH

www.elsevier.nl/locate/jcrysgro

# Growth of high quality InGaAsN heterostructures and their laser application

A.Yu. Egorov[a,*,1], D. Bernklau[a], B. Borchert[a], S. Illek[a], D. Livshits[b], A. Rucki[c], M. Schuster[c], A. Kaschner[d], A. Hoffmann[d], Gh. Dumitras[e], M.C. Amann[f], H. Riechert[a]

[a] *Infineon Technologies, Corporate Research Photonics, Otto-Hahn-Ring 6, München D-81 730, Germany*
[b] *A.F. Ioffe Physico-Technical Institute, St. Petersburg 194021, Russian Federation, Russia*
[c] *Siemens AG, Corporate Technology, München D-81 730, Germany*
[d] *Technical University of Berlin, IFKP, Hardenbergstr. 36, Berlin D-10623, Germany*
[e] *Technical University of München, Physik Department E16, Garching D-85748, Germany*
[f] *Technical University of München, Walter Schottky Institut, Garching D-85748, Germany*

**Abstract**

Focus of this work is the optimization of growth to achieve high quality laser material for emission at 1.3 μm and beyond. GaAs/GaAsN/InGaAsN heterostructures were grown by solid source molecular beam epitaxy. To achieve optimum crystal quality of InGaAsN heterostructures, growth was followed by a high temperature treatment at about 700°C. The high optical quality of our annealed material is attested by large exciton recombination lifetimes (more than 2 ns). Consequently, a decrease of single quantum well transparency current density down to 100 A/cm$^2$ is found and SWQ lasers with threshold current densities as low as 350 A/cm$^2$ have been made. This represents clearly the lowest laser thresholds reported so far for emission around 1.3 μm from the InGaAsN material system. © 2001 Published by Elsevier Science B.V.

*Keywords:* B1. Nitrides; B2. Semiconducting gallium arsenide; B3. Laser diodes

## 1. Introduction

In the last few years, considerable attention has been devoted to the research on 1.3 μm laser structures grown on GaAs substrates. In particular, the GaInAsN quaternary alloy, proposed by Kondow [1], theoretically allows a large extension of the emission wavelengths and due to an increased conduction band offset (with respect to GaAs) should lead to excellent high temperature laser operation. Most attractively, the realization of 1.3 μm vertical cavity surface emitting lasers (VCSELs) on GaAs is possible by using the well-established AlAs/GaAs distributed Bragg reflector (DBR) techniques [2,3].

*Corresponding author. Tel.: +49-89-2344-5230; fax: +49-89-2345-3294.

*E-mail address:* henning.riechert@infineon.com (H. Riechert).

[1] On leave from A.F. Ioffe Physico-Technical Institute, St. Petersburg 194021, Russian Federation, Russia.

0022-0248/01/$ - see front matter © 2001 Published by Elsevier Science B.V.
PII: S0022-0248(01)00764-3

At present, the best InGaAsN based broad area lasers demonstrate threshold current densities lower than 0.8 kA/cm$^2$ at 1.3 μm in continuous wave (CW) operation [4,5]. Alternatively, using InAs/GaAs quantum dots as active material, 1.3 μm lasing operation with very low threshold current density (about 100 A/cm$^2$) was reported [6].

## 2. Experimental procedure

The samples studied were grown by solid source molecular beam epitaxy (MBE) on GaAs (0 0 1) substrates in As-rich growth conditions. The substrate temperature was measured by pyrometer. A radio frequency (RF)-coupled plasma source was used to create reactive nitrogen radicals from $N_2$. The computer control was used for the ignition of the RF plasma to have reproducible growth conditions and to minimize the time of establishment of stable plasma operation. The time delay between the moment of plasma ignition and stable operation was about 300 s.

## 3. GaAsN and InGaAsN bulk materials

To investigate the process of nitrogen incorporation in GaAsN and the influence of nitrogen mole fraction on the band gap of GaAsN, a number of samples with nitrogen mole fraction up to 3.5% and a thickness of about 0.2 μm was grown under different growth conditions, varying substrate temperature and varying fluxes of Ga and As. The condition for the RF plasma and the flux of reactive nitrogen radicals remained constant.

The optimal growth temperature range was found to be 440°C–470°C. The increase in growth temperature leads to decreasing nitrogen incorporation and degradation of surface morphology and crystal quality. The decrease in growth temperature lower than 440°C leads to a decreased efficiency of radiative recombination, as is common for any MBE grown material.

As was defined, the nitrogen mole fraction in the grown layer depends on the fluxes of reactive nitrogen radicals, gallium and arsenic and can be described by the following expression:

$$[N] = (F_N - F_N^R)/F_{Ga}, \quad (1)$$

$$F_N^R = F_N k \ln(F_{As}/F_N + 1), \quad (2)$$

where $F_N, F_N^R, F_{Ga}, F_{As}$ are the fluxes of reactive nitrogen, evaporated reactive nitrogen, Ga and As, respectively, and $k$ is the numeric factor (As–N interaction parameter).

The experimental data for nitrogen incorporation are presented in Fig. 1. Fig. 1a shows the nitrogen content as a function of As to N flux ratio at constant flux of N and Ga fluxes corresponding to a growth rate of 1.11 and 2.72 Å/s at a substrate temperature of 440°C. The experimental data were approximated by the function

$$[N] = 0.044/V_{GR}(1 - 0.0255 \ln(F_{As}/F_N + 1)), \quad (3)$$

where $V_{GR}$ is the growth rate in angstrom per second, $F_{As}$ is normalized per $F_{As}^o$ which corresponds to the border between Ga-rich and As-rich growth conditions.

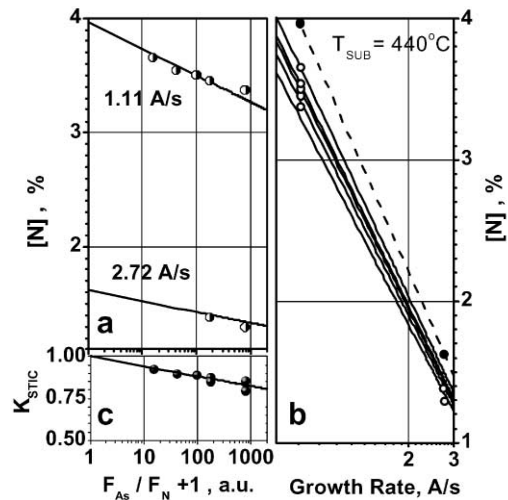


Fig. 1. Nitrogen incorporation into GaAsN at substrate temperature 440°C: (a) Nitrogen alloy content as a function of As to N flux ratio at constant flux of N and Ga correspond to growth rates 1.11 and 2.72 A/s; (b) Nitrogen alloy content as a function of growth rate at constant N-flux (straight lines correspond to the different As to N flux ratio; maximum possible nitrogen alloy content corresponding to zero As-flux is presented by the upper dot line); (c) Sticking coefficient of reactive nitrogen, $K_{STIC}$, versus As to N flux ratio.

Fig. 1b shows the nitrogen content as a function of growth rate (Ga-flux) at constant N-flux. The different lines correspond to different ratios of As and N flux. The maximum possible nitrogen content (corresponding to growth of GaN in Ga-rich growth at zero As-flux, which would be non-stoichiometric material) is presented by the upper dotted line.

Fig. 1c shows the sticking coefficient of reactive nitrogen, $K_{STIC}$, versus As to N ratio. The expression for the sticking coefficient is defined as follows:

$$K_{STIC} = (F_E - F_N^R)/F_N. \quad (4)$$

As can be seen, the sticking coefficient decreases with increasing As to N flux ratio.

To investigate the dependence of the band gap energy of tensile-strained GaAsN and InGaAsN alloys lattice-matched to GaAs on the nitrogen content, a number of samples was grown under constant ratio of group V fluxes and varied growth rate. The dependence of the band gap energy for tensile-strained GaAsN alloys on GaAs (circles, curve (i)) and InGaAsN alloys (triangles) versus nitrogen content at 300 K is presented in Fig. 2a. The curve (ii) presents the band gap energy of quaternary InGaAsN alloys lattice-matched to GaAs. The dotted line corresponds to unstrained GaAsN alloys. The band gap energy was determined from the peak of the photoluminescence (PL) spectra and the nitrogen content was measured by X-ray diffraction.

The bowing parameter of the band gap energy of GaAs–GaN material system was estimated from curve (i) for tensile-strained dilute GaAsN alloy and is presented in Fig. 2b. One can see that the bowing, starting from a value of 25 eV, decreases rapidly with an increase in nitrogen content. For $GaAs_{0.9655}N_{0.0345}$ the bowing parameter is estimated as 12.5 eV.

Usually, GaAsN alloys exhibit weak PL at room temperature as compared to GaAs. No considerable decreasing of PL intensity in the range of nitrogen content of 1%–3.5% was observed. The PL spectra of $GaAs_{0.9655}N_{0.0345}$ recorded at 300 and 77 K are presented in Fig. 3. The PL peak exhibits inhomogeneous broadening of 70 and 30 meV, at 300 and 77 K, respectively, which is typical for GaAsN alloys. An increase in band gap energy of about 60 meV with a decrease of temperature from 300 to 77 K was found, which is somewhat lower than the typical value for the InGaAs material system. It should be mentioned

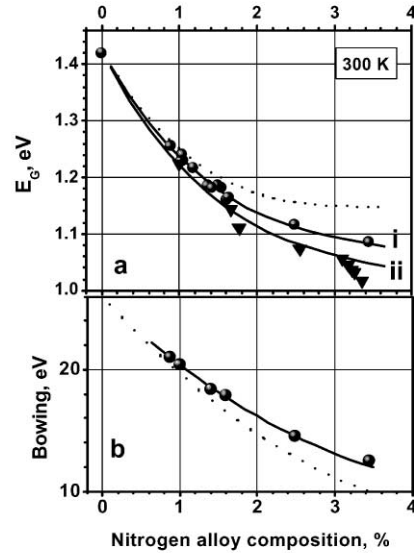


Fig. 2. (a) Band gap energy for tensile-strained GaAsN alloys on GaAs (circles, curve (i); dotted line—unstrained GaAsN alloys) and InGaAsN strain compensated alloys (rhombs) versus nitrogen alloy content at 300 K, curve (ii) presents the band gap energy of quaternary InGaAsN alloys lattice matched to GaAs; (b) Bowing parameter of band gap energy of GaAs–GaN material system for tensile-strained dilute GaAsN alloys (dotted line—unstrained GaAsN alloys).

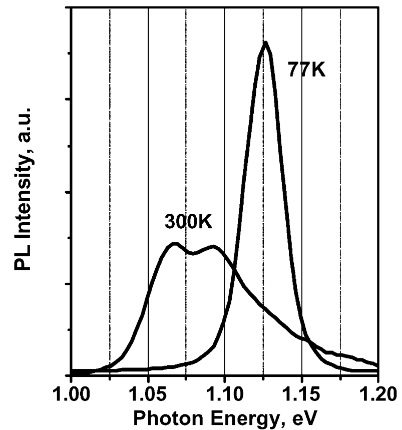


Fig. 3. Photoluminescence spectra of $GaAs_{0.9655}N_{0.0345}$ bulk layer at 77 and 300 K.

that the PL intensity of roughly lattice-matched InGaAsN alloys is higher by one order of magnitude.

## 4. (In,Ga)(As,N) quantum well (QW) heterostructures

Focus of our work was the optimization of growth to achieve high quality laser material for emission at 1.3 μm and beyond. A large number of QW heterostructures was grown to investigate optimal growth conditions. As has been reported, the growth temperature strongly affects the characteristics of InGaAsN [7,8][2]. The optimal temperature for growth of InGaAsN QW heterostructures lies at 470°C and below. The optimum temperature range was defined as 420°C–440°C, which is lower than that of GaAsN alloys and might be as low as 400°C under the cleanest conditions of the growth environment. A considerable increase in PL intensity and decrease in line width for structures grown at lower temperature was found, as shown in Fig. 4. We assume that this behavior is due to the formation of clusters in the QW material during growth at high growth temperature, which leads to the formation of the areas with different localization energy.

To achieve optimum crystal quality of InGaAsN heterostructures, growth must be followed by a high temperature treatment at about 700°C–750°C, for 10–20 min. This typically increases the PL intensity by a factor of 10–20, but also results in a blue shift by about 40–60 nm. Furthermore, the full width at half maximum (FWHM) of PL is slightly reduced to about 25 meV (at 77 K) and in temperature shift of the PL peak due to the temperature coefficient of the band gap from 300 to 77 K increases to about 65 meV. We conclude that the effect of a high temperature treatment is the dissociation of areas with lower localization energy in the QW. We assume that this happens by the dissociation of indium enriched areas (i.e. the rearrangement of indium atoms to give a more uniform distribution) mediated by the presence of N atoms, in analogy to the dissociation of indium enriched areas of self-assembled InAs quantum dots in GaAs matrix during annealing. In this process, the QW becomes more uniform and demonstrates the typical temperature behavior, which now is close to the behavior of an ideal QW heterostructure.

[2] For Ref. [7] correspond to Livshits and Ustinov. Tel.: +049-089-234-45469; fax: +049-089-234-53294; e-mail: mbe@infineon.com.

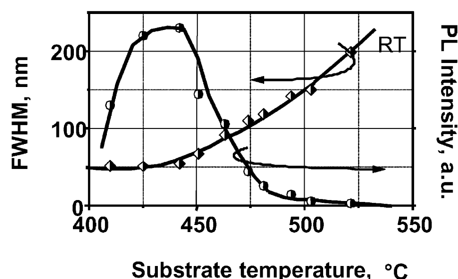


Fig. 4. Influence of growth temperatures on PL characteristics of InGaAsN/GaAs heterostructures.

The changes in PL behavior are accompanied by the appearance of well pronounced structures of QW levels in absorption spectra, as recorded by the photo-deflection spectroscopy (PDS) method at room temperature. The comparison of PDS spectra for QW structure before and after annealing is shown in Fig. 5.

The high optical quality of our annealed material is attested by large exciton recombination lifetimes, which may be more than 2 ns, whereas poor quality samples can demonstrate exciton recombination lifetimes as low as 100–200 ps.

No noticeable effect of V/III ratio in the range from 10 to 2 on material quality, (except for the above-mentioned red shift of PL, due to increase in nitrogen content) was detected.

The comparison of room and low temperature PL of $GaAs/In_{0.2}Ga_{0.8}As_{0.983}N_{0.017}/GaAs$ and $GaAs/In_{0.3}Ga_{0.7}As_{0.972}N_{0.028}/GaAs$ QW of 6.2 nm thick QW samples grown in optimal substrate temperature range after temperature treatment at 740°C for 10 min is shown in Fig. 6. The FWHM of PL spectra 25 and 40 meV was observed at 77 and 300 K, respectively, for an $In_{0.2}Ga_{0.8}As_{0.983}N_{0.017}$ QW sample. The temperature shift of the transition energy due to the temperature coefficient of the band gap from 300

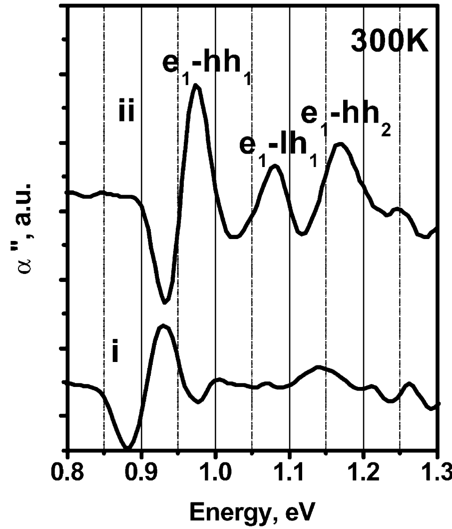


Fig. 5. Absorption spectra of InGaAsN QW heterostructure at 300 K (second differential of the absorption coefficient extracted from PDS spectra): (i) as-grown at 430°C; (ii) after annealing at 720°C for 10 min.

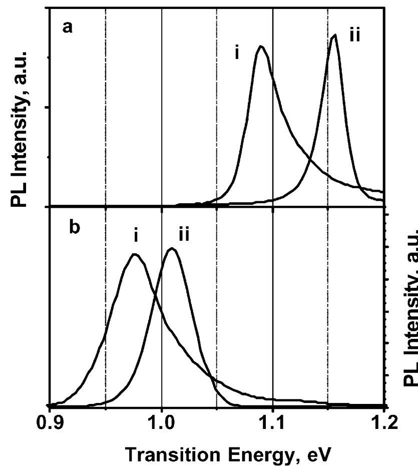


Fig. 6. PL behaviors of InGaAsN QW heterostructures at 300 K (i) and at 77 K (ii): (a) QW GaAs/$In_{0.2}Ga_{0.8}As_{0.983}N_{0.017}$/GaAs of 6.2 nm thick; (b) QW GaAs/$In_{0.3}Ga_{0.7}As_{0.972}N_{0.028}$/GaAs of 6.2 nm thick.

to 77 K was about 65 meV. The FWHM of PL spectra 45 and 65 meV was observed at 77 and 300 K for an $In_{0.3}Ga_{0.7}As_{0.972}N_{0.028}$ QW sample. Obviously, an increase in nitrogen content as well as indium content or increasing growth temperatures leads to the decomposition of the QW material and formation of areas with different localization energy and to a broadening of PL spectra. At 77 K, all carriers are collected in the areas with lower localization energy and the spectral peak shifts to lower energy. This leads to a decreased temperature shift of the PL peak, as compared to QWs with lower indium and nitrogen content, by up to 35 meV. A decrease in growth temperature helps to suppress this phenomenon, leading to a decrease in PL line width and increase in temperature shift.

The ground state transition energy for different GaAs/InGaAsN/GaAs QW heterostructures after temperature treatment at 740°C during 10 min is shown in Fig. 7. Fig. 7 presents the transition energy for GaAs/$GaAs_{(1-x)}N_x$/GaAs and GaAs/$In_{0.3}Ga_{0.7}As_{(1-x)}N_x$/GaAs QW heterostructures versus nitrogen content (QW thickness is 6.2 nm). One can see that 1.275 μm room temperatures emission can be reached with $In_{0.3}Ga_{0.7}As_{0.972}N_{0.028}$ QWs of 6.2 nm thickness. The same transition energy is detected for $In_{0.36}Ga_{0.74}As_{0.981}N_{0.019}$ QWs of 6.5 nm thickness. The PL intensity of $In_{0.36}Ga_{0.74}As_{0.981}N_{0.019}$ QWs heterostructure is higher by a factor 1.5 as compared to $In_{0.3}Ga_{0.7}As_{0.972}N_{0.028}$ QWs.

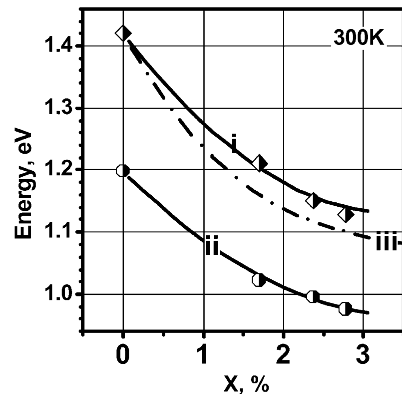


Fig. 7. The ground state transition energy for different QW heterostructures after temperature treatment at 740°C during 10 min: (i) dependence of the transition energy for GaAs/$GaAs_{(1-x)}N_x$/GaAs QW heterostructures versus nitrogen content (QW thickness is 6.2 nm); (ii) dependence of the transition energy for GaAs/$In_{0.3}Ga_{0.7}As_{(1-x)}N_x$/GaAs QW heterostructures versus nitrogen content (QW thickness is 6.2 nm); (iii) band gap of tensile-strained GaAsN on GaAs.

The PL intensity of annealed QW heterostructures is about two orders of magnitude higher as compared to bulk GaAsN alloys.

## 5. Laser application

The active regions of the lasers are based on an InGaAsN QW heterostructure, which is symmetrically inserted into a 300 nm thick, undoped GaAs cavity. The p- and n-type cladding layers consist of 1.5 μm thick $Al_{0.35}Ga_{0.65}As$, doped with Be and Si to $1\text{–}6\times10^{17}$ and $5\text{–}9\times10^{17}\,cm^{-3}$, respectively. The 0.6 μm thick p-type GaAs contact layer is doped to about $1\times10^{19}\,cm^{-3}$ in the top 200 nm.

### 5.1. Broad area lasers

Conventional photolithography and wet etching were used to fabricate broad area devices with 100 μm stripe width. Devices were mounted p-side down onto copper heatsinks using indium solder.

The characteristics of broad area lasers measured in pulsed operation (pulse width $\tau = 2\,\mu s$ and repetition frequency $f = 5\,kHz$) with different active regions are compared in Table 1. The active regions of the presented laser diodes are based on single (SQW), double (DQW) and triple (TQW) InGaAsN QW heterostructures with GaAs, GaAsN or InGaAsN barriers. The In mole fraction of QW material was about $36\pm1\%$, nitrogen mole fraction $1.8\pm0.1\%$. The QW thickness was varied in the range 6.2–6.8 nm.

It should be mentioned that the lowest threshold current density of $350\,A/cm^2$ was obtained for a SQW laser with cavity length of 800 μm based on an GaAsN/InGaAsN/GaAsN QW active region.

For CW measurements, the front and back facets were coated with dielectric antireflection and high reflection coatings of 5% and 99% reflectivity. Special care was devoted to the coating process in order to prevent deposition of the dielectric onto the p-contact in the very vicinity of the laser facets, which would reduce the thermal conductivity of the near facet regions. The SQW laser (2000 × 100 μm) demonstrates a slope efficiency of 0.58 W/A and a threshold current of 670 mA [3]. The highest light output power of 8 W at a current of 15.5 A was observed when stabilizing the laser active region temperature at 10°C and corresponds to a front facet power density of about $30\,MW/cm^2$ (lasing wavelength 1300 nm). Even at this power density, no catastrophic optical mirror damage (COMD) was observed. When stabilizing the heat sink temperature to 10°C, the highest CW output power obtained is 4.2 W, which was limited by excessive heating of the laser chip.

Table 1
InGaAsN lasers

| Active region | Growth method | Threshold current density ($kA/cm^2$) | $\lambda$ (nm) | Slope eff. (W/A) | $T_0$ (K) |
|---|---|---|---|---|---|
| *Broad area lasers 800 × 100 μm* | | | | | |
| SQW InGaAsN (6.8 nm) CaAsN barriers | MBE | 0.51 | 1285 | 0.22 | 60 |
| SQW InGaAsN (6.2 nm) CaAsN barriers | MBE | 0.35 | 1270 | 0.25 | 65 |
| SQW InGaAsN (6.2 nm) CaAs barriers | MBE | 0.54 | 1260 | 0.24 | 83 |
| DQW InGaAsN (6.5 nm) InCaAsN barriers | MBE | 0.63 | 1295 | 0.25 | 75 |
| TQWs InGaAsN (6.2 nm) InCaAsN barriers | MBE | 0.65 | 1290 | 0.23 | 77 |
| InP-reference laser 5 QW (6 nm) | MOCVD | 0.50 | 1300 | 0.22 | 60 |
| *Ridge-waveguide Lasers* | | Threshold current (mA) | | | |
| TQWs (6.2 nm) 300 × 2.5 μm, HR coated mirrors | MBE | 11 | 1280 | 0.39 | 90 |
| TQWs (6.2 nm) 350 × 4 μm, as-cleaved | MBE | 16 | 1295 | 0.24 | 78 |
| DQWs (6.5 nm) 700 × 4 μm, as-cleaved | MBE | 31 | 1295 | 0.21 | 110 |

A preliminary lifetime test was carried out at a CW light output power of 1.5 W and a heat sink temperature of 35°C. After 3000 h no noticeable degradation was observed.

### 5.2. Ridge-waveguide lasers

The narrow stripe (2.5 – 4 μm) ridge-waveguide (RWG) lasers were processed by Ar ion etching technique from DQW and TQW heterostructures and mounted p-side up. A typical pulsed light output power – current curve for a $350 \times 3.5$ μm as a cleaved device fabricated from a TQW structure is shown in Fig. 8 for heat sink temperatures of 25°C, 40°C, 60°C and 80°C. Threshold currents at room temperature of 16 mA and a differential efficiency of 0.24 W/A per facet verify the excellent performance of the active material. High frequency small signal modulation characteristics of such a laser demonstrate the potential for high speed operation of these devices. A 3 dB bandwidth of 6.5 and 9.5 GHz at CW power levels of 5 mW (50 mA) and 14 mW (100 mA) were measured, respectively.

Performance data demonstrated with InGaAsN based devices prove that this new material can match the performance of the well matured InGaAsP/InP system.

### 5.3. Temperature characteristics of InGaAsN lasers

The band-offsets between InGaAsN and GaAs are larger than in the conventionally used InGaAsP/InP system, which should allow a greatly improved high-temperature performance of 1.3 μm lasers [1]. The characteristic temperature $T_0$ as high as 170 K was predicted. The first InGaAsN lasers have demonstrated high value of $T_0 = 126$ K ($400 \times 20$ μm), which was accompanied by the high threshold current density of more than 1.8 kA/cm$^2$ [1]. The characteristic temperatures for our low threshold broad area lasers are presented in Fig. 9. Fig. 9 shows $T_0$ as a function of the total laser loss $\alpha$, which is defined by the expression

$$\alpha = \alpha_i + 1/L \ln(1/R) \tag{5}$$

($\alpha_i$, $L$, $R$ are internal loss, laser length, mirror reflectivity), for the lasers with threshold current density lower than 500 A/cm$^2$ per QW. The laser length, $L$, is varied. One can see that the characteristic temperatures are much lower than those predicted. The maximum possible values of $T_0$ (intrinsic value) corresponding to characteristic temperatures for transparency current at $\alpha = 0$ are about 90–100 K for QW with GaAsN barriers and 100–110 K for QW with GaAs barriers. These values decrease with the decrease in laser length. The RWG lasers usually demonstrate a higher value of $T_0$ than broad area lasers of the same length.

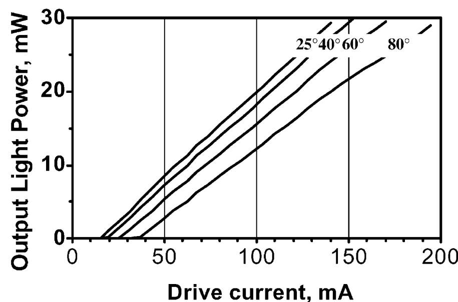


Fig. 8. Output light power–current curves for a $350 \times 3.5$ μm cleaved device fabricated from a TQW structure at different temperatures (pulsed operation).

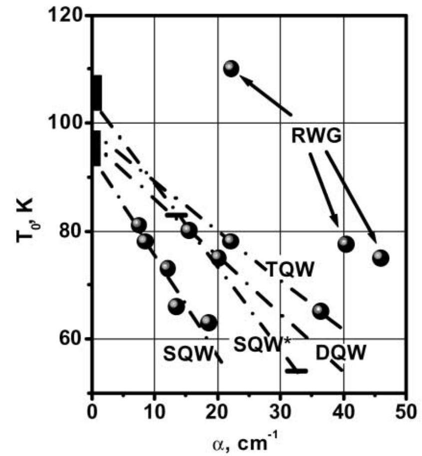


Fig. 9. The characteristic temperatures $T_0$ of low threshold InGaAsN lasers as a function of total laser loss $\alpha$ (SQW—InGaAsN QW with GaAs barriers).

## 6. Conclusion

In conclusion, the characteristics of (In,-Ga)(As,N) bulk materials and QW heterostructures up to 3.5% nitrogen alloy content were investigated and the influence of MBE growth conditions on material quality was defined. High quality InGaAsN QWs corresponding to highest efficiencies of radiative recombination exhibit a low FWHM of the PL peak (25–30 meV, at 77 K), a temperature shift of PL spectrum by about 65 meV and an exiton recombination lifetime of more than 2 ns.

Low threshold and high power operation of InGaAsN QW lasers were demonstrated with characteristic temperatures of about 60–110 K. The lowest threshold current density and highest output power were observed for lasers based on a GaAsN/InGaAsN/GaAsN SQW active region.

## Acknowledgements

A.Yu. Egorov gratefully acknowledges support by an A.v. Humboldt fellowship. This work was partly funded by the EU under BriteEuram BRPR-CT98-0721 (OPTIVAN).

## References

[1] M. Kondow, T. Kitatani, S. Nakatsuka, M.C. Larson, K. Nakahara, Y. Yazawa, K. Uomi, IEEE J. Sel. Topics Quantum Electron. 3 (1997) 719.

[2] J.A. Lott, N.N. Ledentsov, V.M. Ustinov, N.A. Maleev, A.E. Zhukov, A.R. Kovsh, M.V. Maximov, B.V. Volovik, Zh.I. Alferov, D. Bimberg, Electron. Lett. 36 (5) (2000) 1384.

[3] K.D. Choquette, J.F. Klem, A.J. Fischer, O. Blum, A.A. Allerman, I.J. Fritz, S.R. Kurtz, W.G. Breiland, R. Sieg, K.M. Geib, J.W. Scott, R.L. Naone, Electron. Lett. 36 (5) (2000) 1388.

[4] F. Höhnsdorf, J. Koch, S. Leu, W. Stolz, B. Borchert, M. Druminski, Electron. Lett. 35 (7) (1999) 571.

[5] D. Livshits, A.Yu. Egorov, H. Riechert, Electron. Lett. 36 (5) (2000) 1381.

[6] M. Maximov, Yu. Shernyakov, I. Kaiander, D. Bedarev, E. Kondrateva, P. Kopev, A. Kovsh, N. Maleev, S. Mikhrin, A. Tsatsulnikov, V. Ustinov, B. Volovik, A. Zhukov, Zh. Alferov, N.N. Ledentsov, D. Bimberg, Electron. Lett. 35 (23) (1999) 2038.

[7] A.Yu. Egorov, D. Bernklau, D. Livshits, V. Ustinov, Zh.I. Alferov, H. Riechert, Inst. Phys. Ser. 166; pp. 359–362 (Chapter 6). Paper presented at 26th International Symposium on Compound Semiconductors, Berlin, Germany, 22–26 August 1999.

[8] T. Kageyama, T. Miyamoto, S. Makino, F. Koyama, K. Iga, Jpn. J. Appl. Phys. 38 (1999) L298.